Volcán Tancítaro, Michoacán, Mexico, $^{40}Ar/^{39}Ar$ constraints on its history of sector collapse

Steven Ownby [a,*], Hugo Delgado Granados [b], Rebecca A. Lange [a], Chris M. Hall [a]

[a] *Department of Geological Sciences, University of Michigan, Ann Arbor MI, 48109-1063, USA*
[b] *Instituto de Geofisica, UNAM, 0410 DF Coyoacan, Mexico*

Abstract

Volcán Tancítaro is a 97 ± 3 km^3 stratovolcano located in the Michoacán Guanajuato volcanic field (MGVF), part of the Trans Mexican Volcanic Belt. Prior to this study, there was only one K–Ar date (530 ± 60 ka; [Ban, M., Hasenaka, T., Delgado-Granados, H., Takaoka, N., 1992. K–Ar ages of lavas from shield volcanoes in the Michoacán–Guanajuato volcanic field, Mexico. Geofisica Internacional 31 (4), 467–473.] and one sector-collapse event reported for this volcano in the literature [Garduño-Monroy V.H., Corona-Chávez, P., Israde-Alcantara, I., Mennella, L., Arreygue, E., Bigioggero, B., Chiesa, S., 1999. Carta Geológica de Michoacán, scale 1:250,000. Universidad Michoacana de San Nicolás de Hidalgo.; Capra, L., Macías, J.L., Scott, K.M., Abrams, M., Garduño-Monroy, V.H., 2002. Debris avalanches and debris flows transformed from collapses in the Trans-Mexican Volcanic Belt, Mexico — Behavior, and implications for hazard assessment. Journal of Volcanology and Geothermal Research 113, 81–110.]. Twenty-six new $^{40}Ar/^{39}Ar$ ages indicate that Volcán Tancítaro became active $\geq 793 \pm 22$ ka and that the most recent effusive activity occurred at 237 ± 34 ka. Two catastrophic sector-collapse events are identified and dated; the first one occurred on the west side between 694 and 571 ka, whereas the second one occurred on the east side between 261 and 238 ka. The older collapse produced a 2.3–3.4 km^3 debris-avalanche and laharic deposit spread over ~ 567 km^2, whereas the more recent collapse left a 3-km wide, horseshoe-shaped scar on the eastern flank and produced a 3.6–7.0 km^3 debris-avalanche and laharic deposit that covers ~ 654 km^2. Reconstruction of the main edifice of Volcán Tancítaro using ArcGIS software and digital elevation models indicates that the volume removed during the eastern sector collapse was ~ 4.7 km^3.

1. Introduction

Volcán Tancítaro is a large (~ 100 km^3) andesitic, composite volcano located in the Michoacán–Guanajuato Volcanic Field (MGVF) in west-central Mexico (Fig. 1). With a height of 3840 m, rising >2000 m above the surrounding landscape, V. Tancítaro is the dominant

feature in the MGVF. In addition to its size and height, the structural setting of V. Tancítaro in a tectonically active region (Connor, 1987; Pacheco et al., 1999) has contributed to its gravitational instability, leading to sector collapses, which have produced debris avalanches and related lahars in its geologic history. This is evidenced by a 3-km wide, horseshoe-shaped scar on its east side (Fig. 2), the presence of debris-avalanche deposits on both the western and southeastern slopes of the volcano, and a wide fan of related laharic deposits on which the surrounding

* Corresponding author. Fax: +1 734 763 4690.
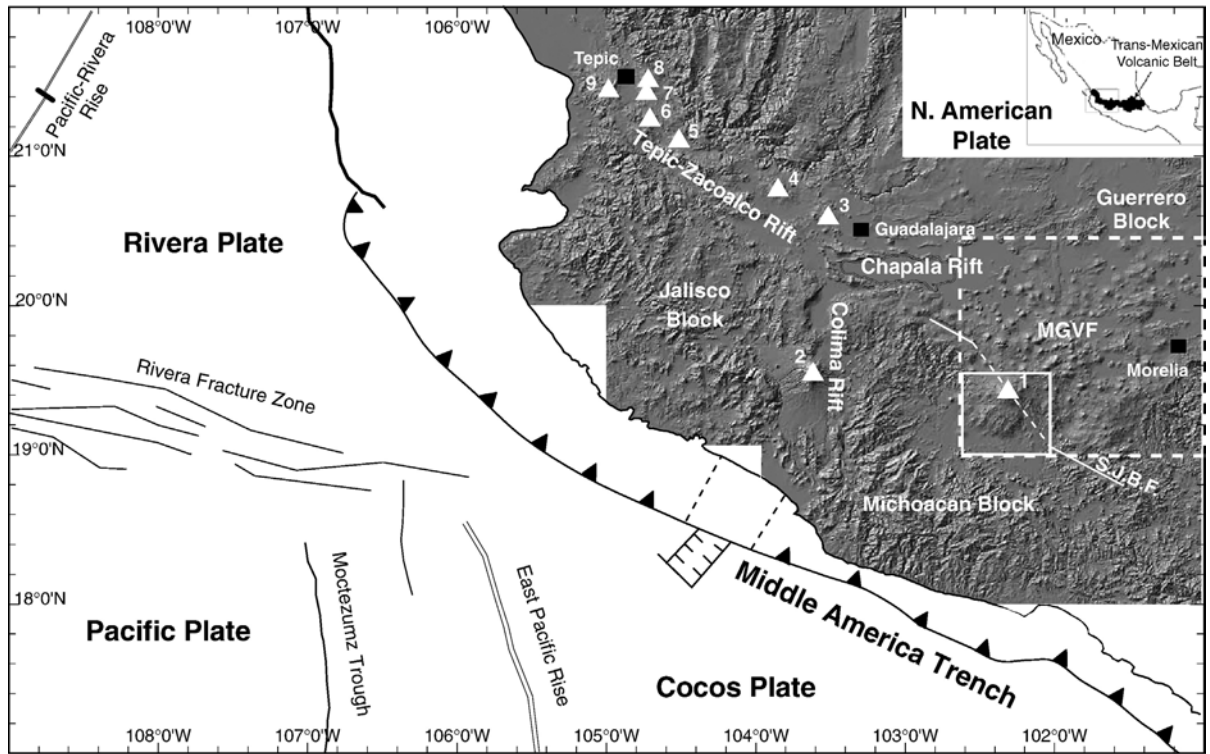 *E-mail address:* sownby@umich.edu (S. Ownby).

Fig. 1. Tectonic overview of western Mexico, modified from Delgado–Granados (1993). Numbered triangles refer to volcanic centers: (1) V. Tancítaro, (2) V. Colima, (3) Sierra La Primavera, (4) V. Tequila, (5) V. Ceboruco, (6) V. Tepetiltic, (7) V. Sangangüey, (8) V. Las Navajas, (9) V. San Juan. S.J.B.F. = San Juanico–Buenavista Fault. The dashed box represents the Michoacán Guanajuato Volcanic Field (MGVF).

communities of Buenavista Tomatlán, Apatzingán, and Nueva Italia reside (Garduño-Monroy et al., 1999; Capra et al., 2002).

Large composite volcanoes like V. Tancítaro have complex histories of growth and collapse, which require detailed geochronology and mapping to fully understand. Stratovolcanoes are built through the accumulation of lava and pyroclastic eruptions, which can be dated by a variety of methods; the most common is $^{40}Ar/^{36}Ar$ geochronology. However, sector-collapse events are difficult to date because juvenile (magmatic) material may be absent or difficult to find within them. In several cases, the associated debris-avalanche deposits are dated by the radiocarbon method applied to organic material entrained during the event (e.g. Brantley and Glicken, 1986; Siebe et al., 1992; Wright, 1998; Belousov et al., 1999; Thouret et al., 2001); however, this approach cannot be applied to deposits that date back several hundred thousand years.

An alternative approach is to apply $^{40}Ar/^{39}Ar$ geochronology to the numerous cinder cones, lava flows, and shield volcanoes that surround V. Tancítaro; these are found both above and below the debris deposits. In recent years, the $^{40}Ar/^{39}Ar$ method has been shown to reliably date lavas <1 Ma (e.g. Hildreth and Lanphere, 1994; Renne et al., 1997; Singer et al., 1997; Frey et al., 2004; Lewis-Kenedi et al., 2005; Jicha and Singer, 2006). Therefore, one goal of this study is to use $^{40}Ar/^{39}Ar$ geochronology to bracket the age of two debris-avalanche deposits derived from sector-collapse events at V. Tancítaro.

A second goal of this paper is to use digital elevation models and Geographic Information Systems (GIS) software to estimate the volume of material involved in the collapse events at V. Tancítaro. The volume of material involved during a sector collapse is one of the most important factors in determining the energy released and the travel distances of the associated debris avalanches and lahars (Iverson, 1997; Iverson et al., 1998). For events <0.1 km^3, flume experiments can be conducted where both the volume of material and the area inundated by a debris flow are well constrained. However, for collapse events at stratovolcanoes involving >1 km^3 of material, researchers must rely on the few well-mapped historical occurrences. The advent of digital elevation models and GIS software allows the study of prehistoric debris-avalanche deposits and an estimate of their volumes, which can be added to the
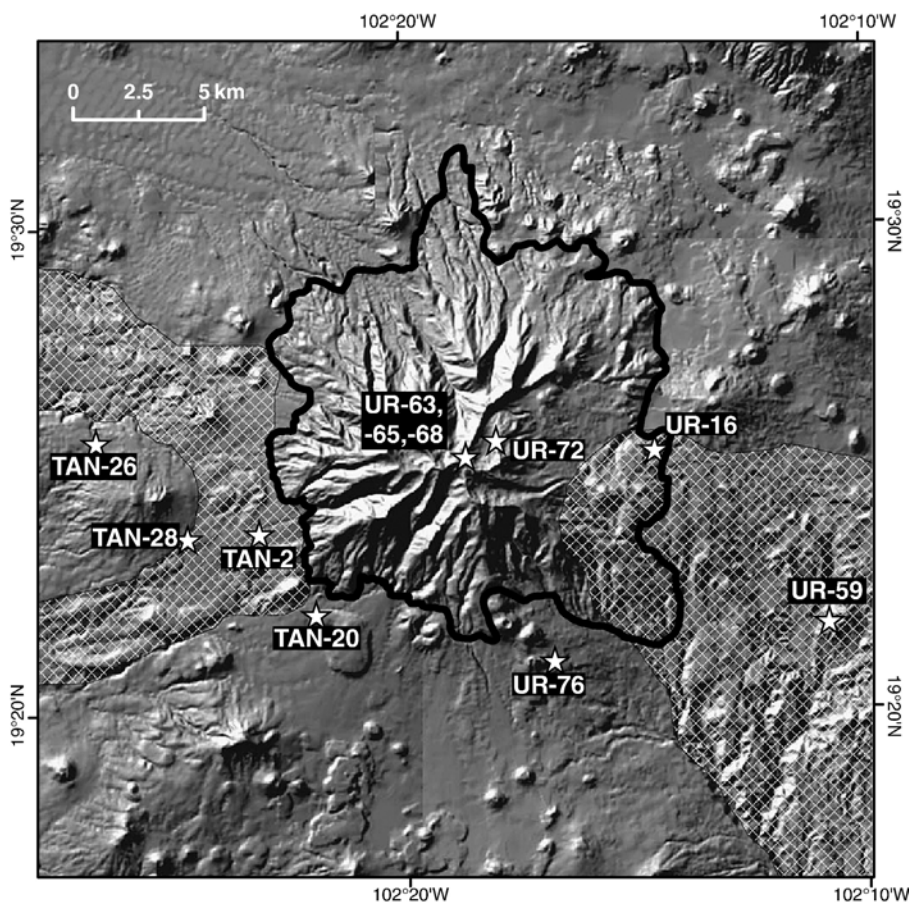
Fig. 2. Shaded relief map of Volcán Tancítaro with sample locations dated in this study. Heavy black line is the outline of V. Tancítaro. Hatched areas are known debris avalanche deposits.

database used to calibrate models that forecast run-out distances of potential debris flows from large volcanic edifices (Iverson et al., 1998). This, in turn, aids the creation of hazards maps for areas surrounding these large composite volcanoes.

2. Tectonic background and structural setting of V. Tancítaro

The Michoacán–Guanajuato Volcanic Field (MGVF) spans an area of ~40,000 km^2 in the central portion of the Trans-Mexican Volcanic Belt (TMVB). The MGVF is notable for the existence of >1000 cinder cones, >300 low-angle shield volcanoes, and two composite volcanoes, the largest of which is Volcán Tancítaro (Hasenaka and Carmichael, 1985; Connor, 1987; Hasenaka, 1994; Hasenaka et al., 1994).

Volcanism in the MGVF is related to the subduction of the Cocos plate beneath the North American plate along the Middle America Trench. The Cocos plate

offshore of Michoacán is ~13 Ma and subducts at a rate of ~5.5 cm/yr, with a 14° dip that steepens to 31° between 25 and 100 km depth (Klitgord and Mammerickx, 1982; NUVEL 1A model of DeMets et al., 1994; Pardo and Suárez, 1995). At depths greater than 100 km, seismicity ceases (Pardo and Suárez, 1995). V. Tancítaro is located ~230 km from the trench and ~120 km above the subducted slab (Pardo and Suárez, 1995). Analysis of Bouguer gravity anomalies from the area suggests that the crustal thickness, along a N–S cross-section at 102° W, is ~30–32 km at the coast and increases to ~40–44 km under the volcanic arc (Urrutia-Fucugauchi and Flores-Ruiz, 1996).

Subduction of the Cocos plate has evolved through time, resulting in a southward migration of the volcanic front of the MGVF, changes in the convergence rate, and variations in the tectonic regime and stress field (Ban et al., 1992; Delgado-Granados et al., 1993, 1995, 1997). The dominant stress field in the MGVF region is characterized by a NE–SW maximum horizontal stress, although the

southern part of the volcanic field is influenced by strike–slip motion associated with the Chapala–Oaxaca fault zone, which may be part of the sliver tectonics related to the convergence of the Cocos and North America plates (Connor, 1987; Delgado-Granados et al., 1995, 1997).

Structurally, V. Tancítaro is located along the NW–SE trending Chapala–Oaxaca fault zone, the boundary between the Michoacán and Guerrero blocks (Fig. 1; Johnson and Harrison, 1990). The segment of this fault adjacent to V. Tancítaro is called the San Juanico–Buenavista fault, which is not well exposed due to extensive Quaternary volcanism. Seismic data from a 1997 earthquake swarm along this NW-trending fault show left-lateral, strike–slip motion at 10–18 km depth (Pacheco et al., 1999). The seismic data also reveal crustal anisotropy in the NE direction, orthogonal to the Chapala–Oaxaca fault zone, which corresponds to the trend in cinder cone alignment and the maximum horizontal stress (Hasenaka and Carmichael, 1985; Connor, 1987). The intersection of these two planes of crustal weakness provides a passageway for large volumes of magma to reach the surface, thus enabling the construction of V. Tancítaro.

3. Description of debris-avalanche and ash deposits

Since the 1980 eruption of Mount St. Helens, many horseshoe-shaped scars on volcanoes around the world have been interpreted as resulting from sector collapse (e.g., Siebert, 1984). The 3-km wide horseshoe-shaped scar on the east side of V. Tancítaro (Fig. 2) is associated with a collapse that spread a debris-avalanche deposit to the southeast (Fig. 3; Garduño-Monroy et al., 1999; Capra et al., 2002). A second collapse produced a debris-avalanche deposit on the western side of V. Tancítaro (Fig. 4), but no corresponding scar is visible on the main edifice, suggesting that it is older than the one that produced the southeastern deposit. A notable feature of both debris sequences is a lack of voluminous juvenile pyroclastic or airfall material. There is, however, a distinctive and widespread yellow–brown ash deposit from V. Tancítaro that provides one of the few stratigraphic markers in this region.

3.1. Southeastern debris-avalanche and laharic deposits

The southeastern debris-avalanche deposit was first identified and described by Garduño-Monroy et al. (1999), Capra et al. (2002). Its morphology is not typical of a young deposit with an abundance of hummocks, but instead it is deeply eroded with only a few preserved hummocks (Fig. 5a). In outcrop, the deposit is well lithified, matrix supported, and composed of mainly silt-

size particles with a reddish hue. The majority of the clasts in the deposit are angular andesite blocks up to three meters in diameter with variable amounts of weathering and alteration. Clasts in the proximal portions of the deposit are found in hummocks and show jigsaw fracturing (Fig. 5b), a classic characteristic of debris-avalanche deposits (Siebert, 1984; Brantley and Glicken, 1986). The transition from the debris-avalanche to the laharic deposit is complex. The location cannot be determined precisely, but it occurs within 10 km of V. Tancítaro and corresponds with a change in slope. After the transition to the debris-flow deposit, a few small red blocks of consolidated ash-flow tuff and black/gray blocks of lava appear as clasts. The ash-flow clasts are presumably from the Sierra Madre Occidental basement, which is exposed in the southern portion of the field area and in the bottom of the canyons in the western portions of the field area (Ownby, unpublished data). The darker lava clasts (basalt through andesite) were likely derived from the cones, shields, and flows that erupted throughout the area over the past million years.

The southeastern laharic deposit is two to ten meters thick. It consists of a sequence of debris-flow deposits and some hyperconcentrated-flow deposits. It is bounded by current drainages and is closely associated with fluvial sediments, located both above and below it (Fig. 5c). The fluvial sediments are pale gray in color and contain well-rounded clasts that are better sorted than those in the laharic deposit. From aerial photographs and field reconnaissance, the laharic deposit terminates a few kilometers south of the town of Nueva Italia ~50 km from V. Tancítaro (Fig. 3). However, it has been reworked into multiple fluvial layers farther south and up to 80 km from V. Tancítaro. These reworked deposits still have the characteristic red coloration, are well lithified, and range up to 3 m thick.

3.2. Western debris-avalanche and related laharic deposits

The western debris-avalanche deposit is similar to the southeastern deposit in that it is well lithified, matrix supported, and contains abundant blocks of jigsaw-fractured andesite up to three meters in diameter in the proximal areas. Scattered around the larger blocks are angular fragments of andesite that range in size down to two centimeters in diameter suspended in a white clay-rich matrix. A few hummocks are preserved as low hills in the proximal portion of the deposit, which are ~10 m thick with rounded tops covered by fragmented andesite (sites TD-8 and TD-29; Fig. 4). One block of lacustrine sediment, 40 cm long was found near the top of one of the
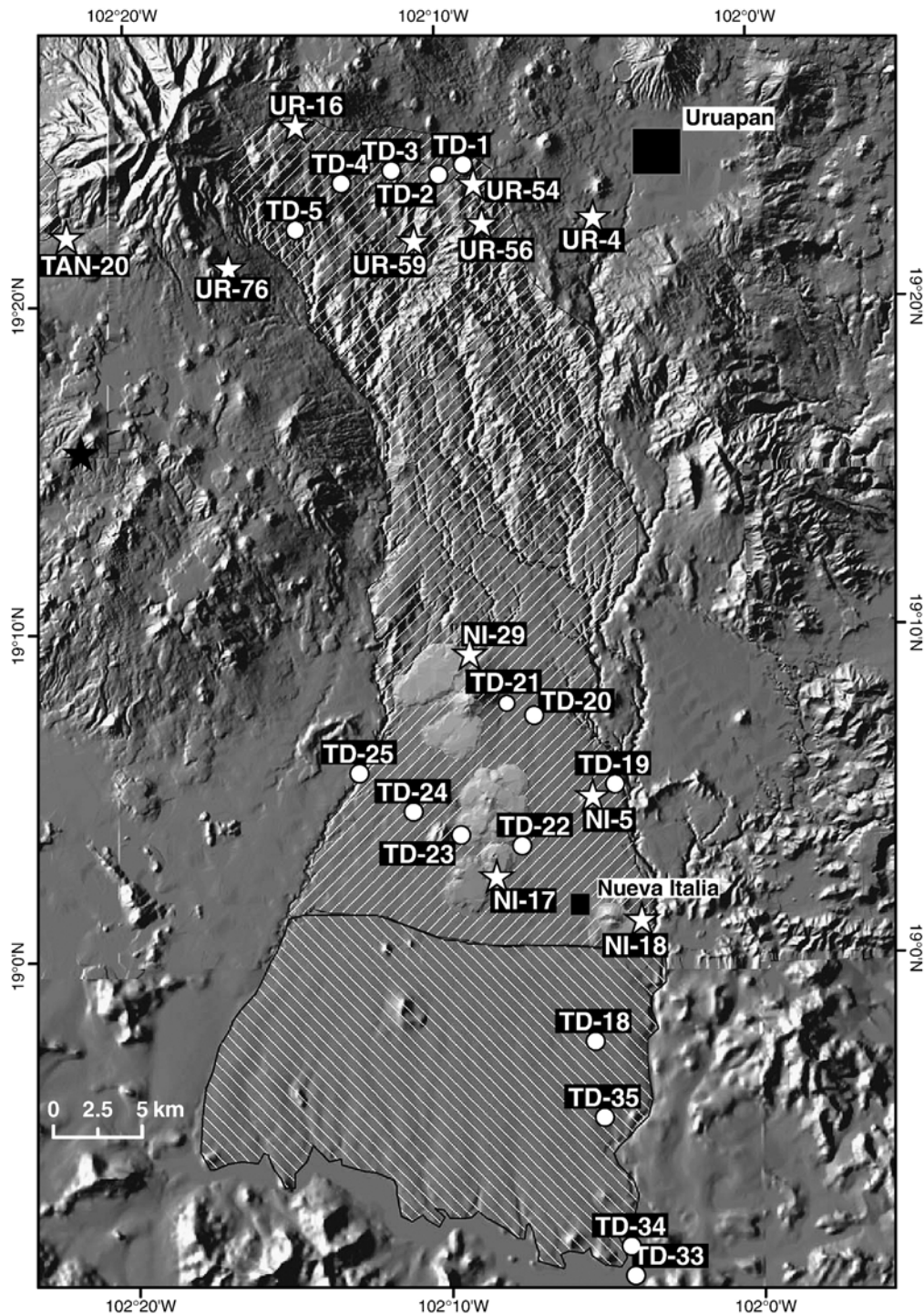
Fig. 3. Map of the southeastern debris avalanche deposit. Hatched area is the maximum inundated area for the deposit with the reversed hatch area being laharic and reworked deposits. Black squares are the cities of Uruapan, and Nueva Italia. White circles are sample locations used for descriptions of the DAD. The white stars are dated sample locations.

hummocks, ~ 18 km from V. Tancítaro (site TD-9; Fig. 4). The debris-avalanche deposit has a complex transition into a laharic deposit that consists of a matrix-supported debris-

flow deposit (one to ten meters in thickness) ~ 20 km from V. Tancítaro. This transitional zone is 1–3 km wide where the debris-avalanche deposit appears and disappears
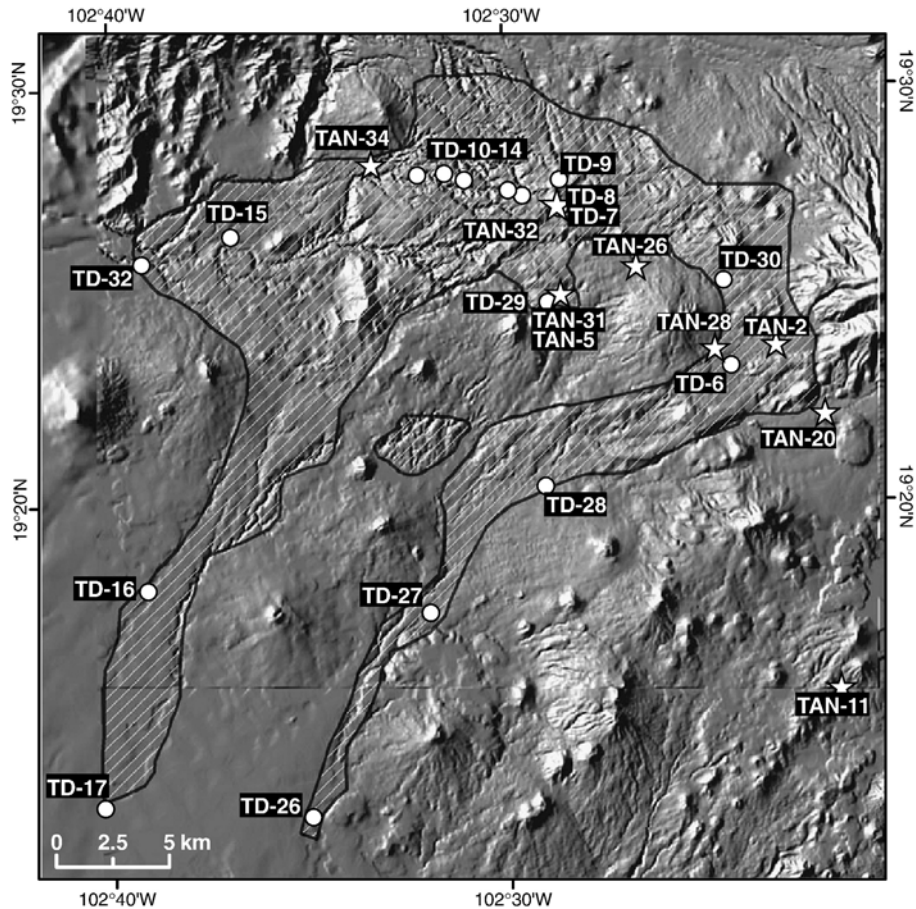
Fig. 4. Map of the western debris avalanche deposit. Hatched area is the extent of the western deposit. White circles are sample locations used for debris-avalanche deposit descriptions. White stars are dated sample locations.

laterally and vertically, covered or uncovered by sequences of debris-flow deposits and/or hyperconcentrated-flow deposits. These secondary deposits are <1 m thick and suggest significant reworking at the transition zone (site TD-10 through TD-14; Fig. 4).

The first sign of aggradations of basement rocks in the deposit occurs ~20 km from V. Tancítaro; these blocks are red ash-flow tuffs and dark lavas (basalt through andesite), similar to the basement clasts found in the southeastern laharic deposits. With increasing distance from V. Tancítaro, outcrops are less abundant and thick, but the deposit is best exposed in riverbanks, road cuts, and gravel quarries. Near its terminus, the debris-flow deposit becomes inter-layered with lacustrine deposits, where each layer is ~1 m thick with four individual debris-flow layers in a single outcrop. It is also intercalated with fluvial deposits at several streams crossed along the road Buenavista–Nueva Italia.

3.3. Yellow–brown ash deposit from Volcán Tancítaro

A distinctive layer of yellow–brown ash, with a thickness between several centimeters and 1–2 m, is found at the summit of V. Tancítaro and throughout the horseshoe-shaped scar region. It is also found on top of many, but not all, peripheral shield volcanoes and fissure-fed flows located east, south, and west of V. Tancítaro. Its yellow–brown color distinguishes it from black ashes from the eruption of nearby cinder cones, such as Parícutin (i.e. Luhr and Simkin, 1993). The characteristics of the yellow–brown ash allow its use as a stratigraphic marker in the surroundings of V. Tancítaro.

4. ^{40}Ar/^{39}Ar chronology

^{40}Ar/^{39}Ar dating was performed at the Argon Geochronology Laboratory at the University of Michigan. A detailed description of the method is found in Frey

et al. (2004). The correlation diagrams and release diagrams are reported in Appendix A. Total gas, plateau, and two isochron ages are reported for each experiment (Table 1). The plateau ages, if available, are preferred and will be used in the following discussion. All errors reported in the text are at the two-sigma level.

4.1. Age constraints on the southeastern debris-avalanche and laharic deposits

Twelve dated lavas provide stratigraphic constraints on the age of the southeastern debris-avalanche and related laharic deposits (Table 1). The most definitive bracket is obtained from dates on three summit lavas (UR-63, UR-65, UR-68) cut by the sector collapse event (thus older) and the resurgent dome (UR-72) that followed (thus younger). The three summit lavas gave plateau ages of 239 ± 26 ka, 254 ± 29 ka, and 209 ± 41 ka, respectively, for an error-weighted average age of 239 ± 22 ka with a MSWD of 1.6. Thus, at the 95% confidence level of these ages, the eastern sector collapse of the volcanic edifice must have occurred after 261 ka (Fig. 6). If the ages of the three lavas are taken individually, then the maximum age for the collapse is 250 ka (maximum date for UR-68). The plateau age for the resurgent dome is 237 ± 34 ka, which indicates that sector collapse must have occurred

earlier than 203 ka, at the 95% confidence level (Fig. 6). The data further indicate that sector collapse occurred close in time to the eruption of the summit lavas, which in turn was closely followed by emplacement of the resurgent dome.

Based only on lavas from V. Tancítaro, the age for the eastern sector-collapse event is between 261 and 203 ka. This age is consistent with the ages obtained on four andesite blocks (UR-16, UR-54, UR-59, and UR-56) found within the southeastern debris-avalanche deposit (and thus older). These blocks gave plateau ages of 305 ± 18 ka, 308 ± 40, 309 ± 62, and 448 ± 18 ka, respectively. Further confirmation is given by dates obtained on lavas overlying the deposit (NI-17, -24 ± 50 ka; NI-29, 82 ± 24 ka; NI-18, 163 ± 37 ka; Table 1 and Fig. 3), which are younger than the age of the resurgent dome. Finally, the age of a cinder cone clearly overlain by the deposit (NI-5, 485 ± 47 ka) indicates stratigraphic consistency among all dated units (Table 1).

4.2. Age constraints on the western debris-avalanche and laharic deposits

Nine dated lavas provide stratigraphic constraints on the age of the western debris-avalanche and laharic deposits (Table 1). Lavas from five shield volcanoes
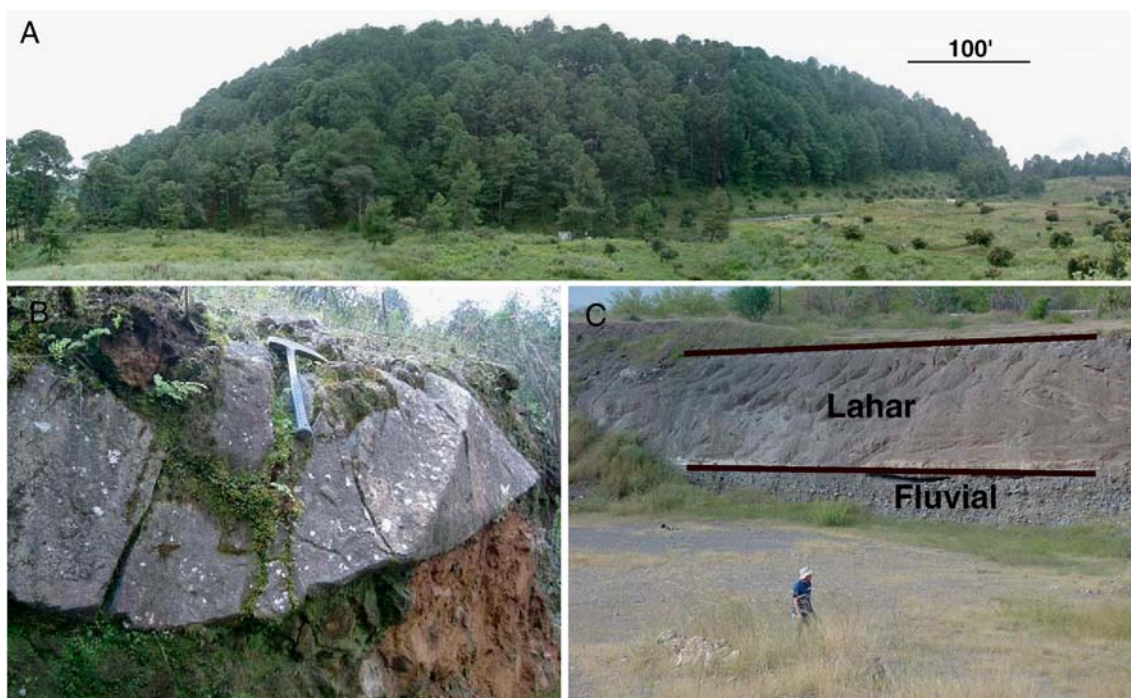

Fig. 5. (A) A hummock made of the southeastern debris-avalanche deposit, (B) jigsaw fracturing in an andesite block from the southeastern debris avalanche deposit, (C) southeastern laharic deposit related to the southeastern debris-avalanche deposit on top of fluvial deposits site TD-34 (see Fig. 3).

Table 1
^{40}Ar/^{39}Ar dates

Sample #	Latitude	Longitude	Notes	Total Gas Age	Plateau age	MSWD	% ^{39}Ar	Steps	Isochron age All pts	MSWD	^{40}Ar/^{36}Ar$_i$	Isochron age Plateau pts	MSWD	^{40}Ar/^{36}Ar$_i$	Pts
NI-17	19°02.36	102°08.47	On top of EDAD	−30±56	−24±50	0.38	91	3–12	179±153	1.07	290.0±3.9	43±207	0.37	293.7±5.5	10
NI-29	19°09.96	102°14.20	On top of EDAD	92±34	82±24	0.77	100	1–13	69±34	0.69	300.5±4.0	69±34	0.69	300.5±4.0	13
NI-18	19°01.02	102°03.09	On top of EDAD	174±43	163±37	0.55	100	1–13	156±44	0.58	297.6±7.4	156±44	0.58	297.6±7.4	13
UR-68	19°25.08	102°18.64	Summit lava	171±55	209±41	0.44	93	2–10	223±47	0.56	285.3±14.8	227±67	0.44	284.0±35.1	9
UR-72	19°25.57	102°17.99	Resurgent dome	247±40	237±34	1.05	86	2–9	251±49	1.36	292.9±21.8	265±46	0.83	275.5±24.4	8
UR-63	19°25.21	102°18.62	Summit lava	250±43	239±26	0.66	98	3–13	228±32	1.18	299.9±5.3	257±40	0.58	288.6±11.7	11
UR-65	19°25.10	102°18.69	Summit lava	251±39	254±29	1.12	93	3–12	241±51	1.12	300.7±17.9	237±56	1.17	303.2±21.0	10
TAN-26	19°25.62	102°26.68	Ash on top	244±27	256±18	0.88	97	3–13	267±23	1.47	290.6±3.6	254±26	0.97	296.2±7.7	11
TAN-28	19°23.63	102°24.72	No ash on top	304±28	269±22	1.32	77	5–10	267±35	2.46	303.5±11.7	298±74	1.44	276.0±48.7	6
UR-76	19°21.03	102°16.78	South flank	301±42	298±29	0.88	92	2–12	300±37	1.12	296.6±9.1	306±34	0.90	291.7±9.6	11
UR-16	19°25.34	102°14.55	Block in EDAD	283±23	305±18	0.54	97	3–13	312±18	0.57	288.2±3.8	310±19	0.38	290.8±6.6	11
UR-54	19°23.49	102°08.88	Block in EDAD	402±63	308±40	0.96	93	4–13	218±102	1.38	305.1±9.1	443±158	0.73	281.4±16.1	10
UR-59	19°21.77	102°10.81	Block in EDAD	286±58	309±62	1.35	91	1–10	381±120	1.97	287.6±5.3	385±86	0.96	287.2±4.0	10
TAN-20	19°22.03	102°21.95	Ash on top	354±34	339±23	0.41	92	2–10	318±57	2.43	327.2±44.6	348±32	0.40	284.7±27.1	9
TAN-10	19°18.94	102°32.31	On top of WDAD	413±78	373±61	0.82	96	3–13	337±82	0.77	298.3±3.9	342±139	0.88	297.8±9.3	11
TAN-11	19°15.44	102°21.64	Ash on top	414±62	385±40	1.14	98	1–12	384±57	1.60	297.6±11.6	393±57	1.24	293.6±14.5	12
UR-4	19°22.43	102°05.06	Ash on top	313±86	429±64	0.34	65	4–9	450±75	0.80	290.3±4.0	371±203	0.33	303.6±26.6	6
TAN-2	19°23.71	102°23.16	Southwest flank	431±31	439±29	0.74	85	6–13	422±57	1.83	297.1±31.5	424±49	0.75	308.8±34.1	8
UR-56	19°22.29	102°08.62	Block in EDAD	426±40	448±18	0.62	100	1–13	452±22	0.48	289.3±4.0	452±22	0.48	289.3±4.0	13
NI-5	19°04.78	102°05.37	Below EDAD	430±48	485±47	1.08	78	7–13	328±124	2.54	299.9±4.8	478±132	1.29	295.7±4.4	7
TAN-39	19°22.62	102°38.72	On top of WDAD	337±62	n.a.				511±223	3.21	289.5±6.9	568±163 [a]	1.48	286.6±5.1	11
TAN-43	19°15.76	102°34.61	On top of WDAD	652±70	612±41	0.94	93	5–13	594±54	0.98	297.1±2.7	607±79	1.07	295.9±5.3	9
TAN-5	19°24.98	102°28.65	Block in WDAD	678±40	673±21	0.49	81	3–8	671±30	1.43	300.8±9.6	650±66	0.49	314.0±49.4	6
TAN-31	19°24.89	102°28.82	Block in WDAD	710±25	728±18	0.71	99	3–13	740±20	0.57	280.5±12.0	743±23	0.44	277.4±19.1	11
TAN-32	19°27.06	102°28.62	Block in WDAD	775±38	793±22	0.97	94.5	3–12	796±24	0.91	284.0±10.9	799±24	0.94	273.7±18.0	10
TAN-34	19°28.12	102°33.35	Below WDAD	1046±34	n.a.				1075±32	3.01	290.9±6.5	1075±30 [a]	2.67	290.4±6.1	11

Notes: All errors are 2σ. WDAD and EDAD denote western and eastern debris-avalanche deposit respectively. Preferred ages are plateau ages.

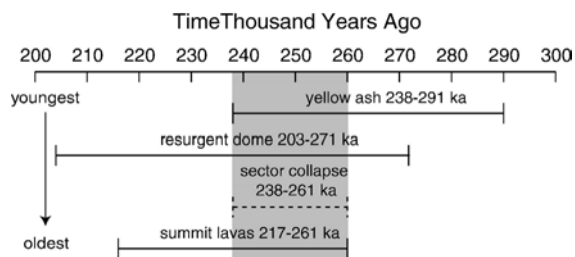[a] No plateau so the isochron based on 11 of 13 steps is preferred.

Fig. 6. Dates used to bracket the age of the eastern sector collapse event.

(TAN-26, -28, -10, -39, and -43) clearly overlie the deposit, whereas one shield (TAN-34; Fig. 4) underlies it. The five lavas on top of the deposit yielded ages of 256 ± 18 ka, 269 ± 22 ka, 373 ± 61 ka, 568 ± 163 ka and 612 ± 41 ka, respectively, whereas the one underneath gave an isochron age of 1075 ± 30 ka. In addition, three andesite blocks (TAN-5, TAN-31, and TAN-32) within the western debris-avalanche deposit (and thus older) gave plateau ages of 673 ± 21 ka, 728 ± 18 ka, and 793 ± 22, respectively. Therefore, the sector-collapse event that occurred on the western side of V. Tancítaro is constrained to have occurred sometime between 673 ± 21 and 612 ± 41 ka (or between 694 and 571 ka, at the 95 % confidence level). These ages are consistent with the lack of a corresponding, visible scar on V. Tancítaro, which has likely been filled by volcanic activity over the last ∼ 600 kyr.

4.3. Age constraints on the yellow–brown ash deposit from Volcán Tancítaro

Ten dated lavas provide stratigraphic constraints on the age of the distinctive yellow–brown ash deposit erupted from V. Tancítaro (Table 1). This distinctive ash is seen in the summit region, throughout the horseshoe-shaped scar region, and on top of the resurgent dome (sample UR-72; 237 ± 34 ka), which means that at least one phase of its eruption occurred after the eastern sector collapse event. The oldest permissible date for the resurgent dome is 271 ka at the 95% confidence level, which indicates that the yellow-ash must have erupted after 271 ka. Additionally, the summit lavas are older than the resurgent dome (cut by the sector collapse event), and therefore the yellow ash on the resurgent dome must be younger than these summit lavas as well. As discussed above in a previous section, their oldest permissible date is 261 ka at the 95% confidence level. Therefore, the yellow ash on the resurgent dome, which must be younger than the summit lavas, is further constrained to be younger than 261 ka. This result is consistent with the occurrence of this yellow–brown ash layer on top of three fissure-fed lava

flows (TAN-20, TAN-11, UR-4) south and east of V. Tancítaro (Fig. 2), with ages of 339 ± 23 ka, 385 ± 40 ka, and 429 ± 64 ka, respectively.

In addition to an upper limit of 261 ka for the eruption of this yellow-brown ash, an age bracket that includes a lower limit comes from its presence and absence on two overlapping shield volcanoes west of V. Tancítaro (Fig. 2). Sample TAN-26 comes from a shield that clearly overlaps (and is thus younger than) the shield immediately to the east, from which sample TAN-28 was taken. The younger shield (TAN-26) gave a date of 256 ± 18 ka and does not have the ash layer on top it, whereas the older shield (TAN-28) gave a date of 269 ± 22 ka and is covered with the yellow–brown ash. From these two shields alone, the eruption of the yellow–brown ash is bracketed to be younger than 291 ka (the oldest permissible age for the older shield at the 95% confidence level) and older than 238 ka (the youngest permissible age for the younger shield at the 95% confidence level). This bracket does not conflict with the maximum age for the yellow–brown ash found on the resurgent dome (261 ka, as outlined above) (Fig. 6). When all the dates that bear on the age of the yellow–brown ash are considered, its eruption is constrained to have occurred between 261 and 238 ka. Moreover, because this ash is found on top of the resurgent dome and throughout the horseshoe-shaped scar area, then at least one phase of its eruption must have occurred after the sector-collapse event. Therefore, the date of the eastern collapse is also bracketed between 261 and 238 ka.

4.4. Additional dates on lavas from Volcán Tancítaro

Two more dates provide additional, though sparse, information on the eruptive history of V. Tancítaro. A flow-banded sample from the southern flank, UR-76, was dated at 298 ± 29 ka, which is similar in age to three andesite blocks (305 ± 18 ka; 308 ± 40 ka; 309 ± 62 ka) found within the eastern debris-avalanche deposits, which are discussed above. In addition, an andesite boulder (TAN-2), three meters in diameter, from the southwestern flank was dated at 439 ± 29 ka and erupted close in time to a block found in the eastern debris-avalanche deposit (UR-56, 448 ± 18 ka).

5. Volume estimates of Volcán Tancítaro and its sector-collapse-related deposits with ArcGIS

ArcGIS is a collection of software products created by ESRI (Environmental Systems Research Institute) for Geographical Information Systems. In this paper the ArcGIS software bundle and digital elevation models

are utilized to create digital maps and calculate the volume of V. Tancítaro as well as the debris-avalanche and laharic deposits. Outlines were created around V. Tancítaro and its associated deposits in ArcGIS with the aid of ortho-airphotos, digital elevation models, and field mapping. Triangulated Irregular Networks (TINs), 3-dimensional representations of the present day topography, were created from each outline. For V. Tancítaro the area under the TIN down to a defined baseline was integrated and a volume calculated via ArcGIS (i.e. Frey et al., 2004; Lewis-Kenedi et al., 2005). Calculation of volumes by this method is not appropriate for the debris-avalanche deposits, which cover large areas with undulating topography; for these deposits an average thickness based on field observations (and error on that thickness) is estimated for their entire area.

5.1. Volume of Volcán Tancítaro

Use of digital elevation models with ArcGIS tools permits the current volume of V. Tancítaro to be calculated, as well as its volume immediately prior to the eastern sector collapse. Hasenaka (1994) estimated the current volume of V. Tancítaro to be ~ 49 km^3 on the basis of 1:50,000 topographic maps with 20 m contour intervals. The digital elevation models and ortho-airphotos allow a more detailed evaluation of the areal extent of the Tancítaro edifice, as well as the sloping baseline beneath it, which leads to a revised estimate of the current volume for V. Tancítaro of $\sim 97 \pm 3$ km^3.

5.2. Volume and length of the southeastern debris-avalanche and laharic deposits

These deposits cover a minimum combined area of 654 km^2 (Fig. 3), which is over three times larger than the previous estimate of 176 km^2 (Garduño-Monroy et al., 1999; Capra et al., 2002). Observed outcrops range between 2 and 10 m thick, which leads to an estimated average thickness of 7 ± 2 m; this is significantly thinner than the average of 20 m previously estimated (Garduño-Monroy et al., 1999; Capra et al., 2002). These estimates of area and thickness yield a minimum and maximum volume of 3.3 and 5.9 km^3 (similar to the previous estimate of 3.52 km^3 of Garduño-Monroy et al., 1999; Capra et al., 2002. The observed run out distance is ~ 60 km with a vertical drop of 3657 m, which yields a height to length (H/L) ratio of 0.06. If the original height of the volcano, prior to sector collapse, was 4450 m (see below), then the H/L ratio changes to 0.07. An additional area of 360 km^2 to the south is covered by fluvial and hyper-concentrated deposits, formed by the reworking

of the debris-avalanche and laharic deposits, that average 2.0 ± 0.5 m in thickness. These reworked deposits add 0.7 ± 0.4 km^3 for a total estimated volume for the material in the original debris-avalanche and laharic deposits that range between 3.6 and 7.0 km^3.

5.3. Volume and length of the western debris-avalanche and laharic deposits

The western debris-avalanche and laharic deposits have together a maximum area of 567 km^2 with an average thickness based on our field observations of $\sim 5 \pm 1$ m. This gives a minimum and maximum volume of 2.3 and 3.4 km^3, respectively. However, the deposit is not exposed over the entire 567 km^2 area, as it is buried under at least five shield volcanoes (Fig. 4). The western debris-avalanche deposit at V. Tancítaro appears to be smaller than the eastern one, with an estimated volume of 2.3–3.4 km^3. This is a minimum estimate of the volume removed from V. Tancítaro because the deposits have been exposed to erosion over the last ~ 600 kyr. Moreover, comparisons with the volume of the resulting scar after the sector collapse more than 600 kyr. ago cannot be made because it has long since been covered by subsequent eruptions. The run-out distance for this deposit is ~ 44 km and the vertical drop from the current summit of V. Tancítaro and the lowest site of deposition is 3460 m for an H/L ratio of 0.08, higher than that for the eastern collapse. However, an ancestral form of V. Tancítaro with an unknown height was the source of this older sequence, so this H/L ratio is only an estimate.

5.4. Volume removed from Volcán Tancítaro during the eastern sector collapse

The volume missing from the horseshoe-shaped scar on the east side of V. Tancítaro was calculated by the difference between the current topography inside the scar and the top of the cliffs that make up the walls of the scar (Fig. 7). The area of the scar is 19.9 km^2, and the missing volume thus calculated is ~ 0.32 km^3. Garduño-Monroy et al. (1999) points out that there is a resurgent dome within the scar (Fig. 2), for which we calculated a volume of ~ 0.15 km^3. With this volume added to the volume of the scar, the new volume of material missing from V. Tancítaro is ~ 0.47 km^3. This missing volume is considerably smaller than the estimate of the volume of deposits discussed above (3.6–7.0 km^3), which suggests that the pre-collapse summit of V. Tancítaro was higher than its current elevation, and that it was likely part of the sector collapse.
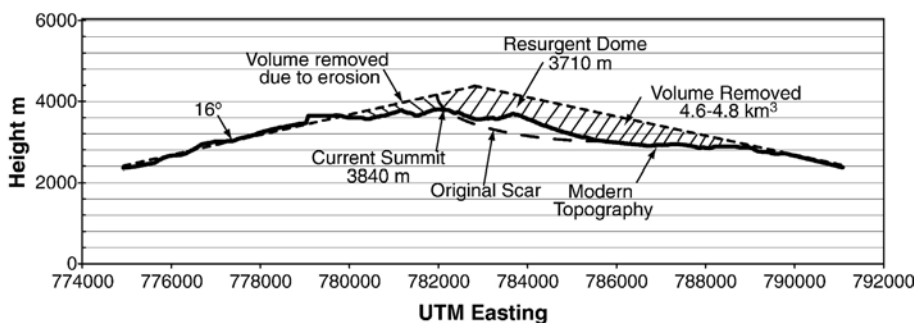
Fig. 7. Cross-section of Volcán Tancítaro with the reconstructed profile.

V. Tancítaro does not currently have a classic conical shape owing to erosion and sector collapse. Furthermore, its highest point is not located at the center of its footprint, but is offset slightly to the west, along the rim of the horseshoe-shaped scar (Fig. 7). If a classical conical shape is reconstructed for V. Tancítaro, then the summit is located between the current summit and the resurgent dome (Fig. 7); therefore, sector collapse likely included the pre-collapse summit region of the volcano, similar to what occurred at Mount St. Helens (southern Washington, USA) in 1980 (Moore and Albee, 1981). The reconstruction of V. Tancítaro was performed by extrapolating the 16° slope of its western side (calculated with the DEM and ArcGIS software) upwards, which leads to a maximum pre-collapse elevation of 4450 m, approximately 610 m higher than the current summit. Hasenaka (1994) calculated a 15° slope for V. Tancítaro on the basis of the topographic map. The volume missing is then approximated by the volume of a cone with the basal area equal to the area of the horseshoe-shaped scar; the height is the difference between the average elevation of the base of the scar and that of the original height of the volcano. This approximation is used because the sector collapse involved only the material directly above the horseshoe-shaped scar from this original structure. Using this method, approximately 4.7 km^3 was removed from V. Tancítaro as a result of the most recent sector collapse. This is consistent with the estimated volume of the southeastern deposits (~ 5.3 km^3), especially when the effects of bulking and dilation are taken into account.

As a test of the method used above to determine the volume of material removed during the sector collapse event, the same method was used to calculate the volume removed during the 1980 sector collapse and eruption of Mount St. Helens. First, the area of the horseshoe-shaped scar on Mount St. Helens was calculated using ArcGIS with the 30 m DEMs. The area calculated is 6.36 km^2, which is larger than the area of the crater floor (1.39 km^2) owing to the removal of the north flank of the volcano

during the collapse. The original height of ~ 2950 m (9677 ft) was then subtracted from the crater floor elevation of ~ 1914 m (6279 ft). The resultant volume missing is 2.19 km^3, which is within 25% of the 2.76 km^3 estimated by Moore and Albee (1981). However, of the 2.76 km^3 removed from Mount St. Helens, only ~ 2.3 km^3 was involved in the debris avalanche because ~ 0.46 km^3 was juvenile material. The ~ 2.3 km^3 volume is within 5% of the material missing (2.19 km^3), based on the calculations in this study using ArcGIS. The ability of the ArcGIS method to reconstruct the volume involved in the well-studied sector collapse at Mount St. Helens suggests that this method can be used to reliably reconstruct volumes of stratovolcanoes and debris-avalanche deposits.

6. Discussion

6.1. History of sector collapse at Volcán Tancítaro

The ^{40}Ar/^{39}Ar geochronology results from this study indicate that an ancestral V. Tancítaro was active ≥ 793 kyr ago, as evidenced by the age of at least one andesite block within the western debris-avalanche deposit. Volcanism continued until the edifice attained sufficient height and mass to undergo sector collapse to the west sometime between 694 and 571 ka. The direction of the collapse roughly coincides with the position of the minimum horizontal stress, a fact that structurally favors sector collapses at other volcanoes (Siebert, 1984; Delgado-Granados, 1999). Whether or not there was a hiatus in eruptive activity at this central vent over the next 200 kyr is not possible to discern with the data presently available, but there was at least one eruption at 439 ± 29 ka. A series of andesite eruptions occurred from V. Tancítaro ~ 300 kyr ago, as three andesite blocks within the southeastern debris-avalanche deposit and one flank flow yielded dates of 305 ± 18 ka, 308 ± 40 ka, 309 ± 62 ka, and 298 ± 29 ka,

respectively. An avalanche scar must have existed on the west side of the ancestral volcano after the sector collapse event between 694 and 571 ka, but subsequent eruptions and construction of the present-day western flank of V. Tancítaro has covered all evidence. This is similar to what is occurring at Volcán Colima today (Fig. 1), where the scar from a sector-collapse event ~4300 yr ago is nearly filled by the new cone of Volcán Colima (Luhr and Prestegaard, 1988; Stoopes and Sheridan, 1992; Capra and Macías, 2002).

The most recent activity at V. Tancítaro was an explosive event, which produced the distinctive yellow–brown ash found on top of the resurgent dome (UR-72), which has been dated at 237 ± 34 ka. At least one phase of the eruption of this yellow ash is constrained to have occurred sometime between 291 and 238 ka, based on its absence and presence on two overlapping shields (TAN-26 and TAN-28, respectively), adjacent to the western flank of V. Tancítaro. This age bracket is close in time to the effusive eruptions of lavas near the present-day summit, which have an error-weighted average age of 239 ± 22 ka. The east side of the volcanic edifice must have collapsed soon after, because the date on the resurgent dome (237 ± 34 ka), which partially filled the horseshoe-shaped scar, is indistinguishable from the dates for the summit lavas. In turn, the distinctive yellow–brown ash, which is found on top of the resurgent dome and throughout the horseshoe-shaped scar region, also must have also erupted soon after the eastern collapse, because it is constrained to have erupted prior to 238 ka (based on it absence on an adjacent shield volcano, TAN-26; Fig. 2).

In summary, the eruption of the summit flows, the collapse of the eastern flank, the emplacement of the resurgent dome, and the eruption of the yellow–brown ash all occurred closely in time, between 261 and 238 ka. This scenario is similar to the history of Mount St. Helens, where at least 25–50% of the volume of the pre-eruptive volcanic edifice (~ 20–40 km^3) was erupted within 4 kyr of the sector collapse event in 1980 (Mullineaux, 1986). Dome growth began immediately after the collapse (Moore et al., 1981) and has continued to the present. In addition, numerous eruptions of ash from Mount St. Helens have occurred prior to and after the 1980 collapse. However, in contrast to events at Mount St. Helens, there is no evidence for any pyroclastic-flow or pyroclastic-fall deposit associated with the eastern sector-collapse event at V. Tancítaro.

Prior to this study, Garduño-Monroy et al. (1999) estimated a Holocene age for the eastern debris-avalanche deposit based on morphological relations between the sector-collapse scar and the glacial valleys along the slopes of V. Tancítaro. They suggested that the sector-collapse event occurred after glacial erosion of the main edifice. However, major glaciations have occurred in North America throughout the Quaternary, and V. Tancítaro has been a topographic high for at least 700 kyr. It has likely undergone many glaciations prior to the most recent one in the Holocene. Therefore a Holocene age for the sector collapse is not required for the Garduño-Monroy et al. (1999) observation of glacial erosion prior to the collapse. Moreover, the resurgent dome appears to have undergone significant erosion, which is clearly visible in the hillshade image (Fig. 2) and is consistent with the ^{40}Ar/^{39}Ar date of 237 ± 34 ka.

7. Conclusions

The use of digital elevation models and ArcGIS software allow for the reconstruction of stratovolcanoes that have undergone prehistoric sector-collapse events by accurately determining the volume of the deposits as well as the volume missing from the main edifice. These volumes can be used in conjunction with high-resolution ^{40}Ar/^{39}Ar geochronology to determine a detailed growth and collapse history for composite volcanoes. These data are essential to better understand the events that lead up to catastrophic sector collapse at stratovolcanoes around the world.

Acknowledgements

Appendix A. Supplementary data

Supplementary data associated with this article can be found, in the online version, at doi:10.1016/j.jvolgeores.2006.10.009.

References

Ban, M., Hasenaka, T., Delgado-Granados, H., Takaoka, N., 1992. K–Ar ages of lavas from shield volcanoes in the Michoacán–Guanajuato volcanic field, Mexico. Geofisica Internacional 31 (4), 467–473.

Belousov, A., Belousova, M., Voight, B., 1999. Multiple edifice failures, debris avalanches and associated eruptions in the Holocene history of Shiveluch volcano, Kamchatka, Russia. Bulletin of Volcanology 61 (5), 324–342.

Brantley, S., Glicken, H., 1986. Volcanic debris avalanches. Earthquakes and Volcanoes 18 (6), 195–206.

Capra, L., Macías, J.L., 2002. The cohesive Naranjo debris-flow deposit (10 km³): a dam breakout flow derived from the Pleistocene debris-avalanche deposit of Nevado de Colima Volcano (Mexico). Journal of Volcanology and Geothermal Research 117, 213–235.

Capra, L., Macías, J.L., Scott, K.M., Abrams, M., Garduño-Monroy, V.H., 2002. Debris avalanches and debris flows transformed from collapses in the Trans-Mexican Volcanic Belt, Mexico — behavior, and implications for hazard assessment. Journal of Volcanology and Geothermal Research 113, 81–110.

Connor, C.B., 1987. Structure of the Michoacán–Guanajuato Volcanic Field, Mexico. Journal of Volcanology and Geothermal Research 33, 191–200.

Delgado-Granados, H., 1993. Late Cenozoic tectonics offshore western Mexico and its relation to the structure and volcanic activity in the western Trans-Mexican volcanic belt. Geofisica Internacional 32, 543–559.

Delgado-Granados, H., 1999. A methodology to evaluate sector-collapse-related hazards at volcanoes and assess disaster prevention planning: the case of central Mexico volcanoes. American Geophysical Union Annual Meeting, December 13–17, pp. F1140–F1141.

Delgado-Granados, H., Urrutia Fucugauchi, J., Hasenaka, T., Ban, M., 1993. Migración del Campo Volcánico de Michoacán - Guanajuato 90 km hacia el suroeste durante los últimos 0.78 Ma. In: Delgado A., Luis, Martín, Arturo (Eds.), Contribuciones a la Tectónica del Occidente de México. Monografía, vol. 1. Unión Geofísica Mexicana, pp. 211–226.

Delgado-Granados, H., Urrutia Fucugauchi, J., Hasenaka, T., Ban, M., 1995. Southwestward volcanic migration in the western Trans-Mexican Volcanic Belt (Mexico) during the last 2 Ma. Special volume on "Comparative Studies on the Tectonics and Volcanism of Circumpacific Arcs", Part B. Geofisica Internacional 34 (3), 341–352.

Delgado-Granados, H., Pacheco, J., Tristán-Serrano, A., Rivera-Cabrera, J.H., 1997. La actividad tectónica del lineamiento Chapala–Oaxaca: evolución geológica del semi-graben de Cotija y sismicidad reciente en la region de Tancítaro–Parícutin. Segundo Congreso Mexicano de Mineralogía, Convención sobre la Evolución Geológica de México, Pachuca Hidalgo.

DeMets, C., Gordon, R.G., Argus, D.F., Stein, S., 1994. Effect of recent revisions to the geomagnetic reversal time scale on estimates of current plate motions. Geophysical Research Letters 21 (20), 2191–2194.

Frey, H.M., Lange, R.A., Hall, C.M., Delgado-Granados, H., 2004. Magma eruption rates constrained by $^{40}Ar/^{39}Ar$ chronology and GIS for the Ceboruco–San Pedro volcanic field, western Mexico. Geological Society of America Bulletin 116 (3/4), 259–276.

Garduño-Monroy V.H., Corona-Chavéz, P., Israde-Alcantara, I., Mennella, L., Arreygue, E., Bigioggero, B., Chiesa, S., 1999. Carta Geológica de Michoacán, scale 1:250,000. Universidad Michoacana de San Nicolás de Hidalgo.

Hasenaka, T., 1994. Size, distribution, and magma output rate for shield volcanoes of the Michoacán–Guanajuato volcanic field, Central Mexico. Journal of Volcanology and Geothermal Research 63, 13–31.

Hasenaka, T., Carmichael, I.S.E., 1985. A compilation of location, size, and geomorphological parameters of volcanoes of the Michoacán–Guanajuato volcanic field, central Mexico. Geofisica Internacional 24 (4), 577–607.

Hasenaka, T., Ban, M., Delgado-Granados, H., 1994. Contrasting volcanism in the Michoacán–Guanajuato Volcanic Field, central Mexico: Shield volcanoes vs. cinder cones. Geofisica Internacional 33 (1), 125–138.

Hildreth, W., Lanphere, M.A., 1994. Potassium–argon geochronology of a basalt–andesite–dacite arc system: the Mount Adams volcanic field, Cascade Range of southern Washington. Geological Society of America Bulletin 106, 1413–1429.

Iverson, R.M., 1997. The physics of debris flows. Reviews of Geophysics 35, 245–296.

Iverson, R.M., Schilling, S.P., Vallance, J.W., 1998. Objective delineation of lahar-inundation hazard zones. Geological Society of America Bulletin 110, 972–984.

Jicha, B.R., Singer, B.S., 2006. Volcanic history and magmatic evolution of Seguam Island, Aleutian Island arc, Alaska. Geological Society of America Bulletin 118, 805–822.

Johnson, C.A., Harrison, C.G.A., 1990. Neotectonics in Central Mexico. Physics of the Earth and Planetary Interiors 64, 187–210.

Klitgord, K.D., Mammerickx, J., 1982. Northern East Pacific Rise: magnetic anomaly and bathymetric framework. Journal of Geophysical Research 87, 6725–6750.

Lewis-Kenedi, C.B., Lange, R.A., Hall, C.M., Delgado-Granados, H., 2005. The eruptive history of the Tequila volcanic field, western Mexico: ages, volumes, and relative proportions of lava types. Bulletin of Volcanology 67, 391–414.

Luhr, J.F., Prestegaard, K.L., 1988. Caldera formation at Volcano Colima, Mexico by a large Holocene volcanic debris avalanche. Journal of Volcanology and Geothermal Research 35, 335–348.

Luhr, J., Simkin, T., 1993. Parícutin: The Volcano Born in a Mexican Cornfield. Geoscience Press, Phoenix, p. 427.

Moore, J.G., Albee, W.C., 1981. Topographic and Structural changes, March–July 1980 — Photogrammetric Data. In: Lipman, P.W., Mullineaux, D.R. (Eds.), The 1980 eruptions of Mount St. Helens. Washington: U.S. Geological Survey Professional Paper, vol. 1250, pp. 347–377.

Moore, J.G., Lipman, P.W., Swanson, D.A., Alpha, T.R., 1981. Growth of Lava Domes in the crater, June 1980–January 1981. In: Lipman, P.W., Mullineaux, D.R. (Eds.), The 1980 Eruptions of Mount St. Helens. Washington: U.S. Geological Survey Professional Paper, vol. 1250, pp. 347–377.

Mullineaux, D.R., 1986. Summary of pre-1980 tephra-fall deposits erupted from Mount St. Helens, Washington State, USA. Bulletin of Volcanology 48, 17–26.

Pacheco, J.F., Valdés-González, C., Delgado, H., Singh, S.K., Zúñiga, R., Mortera-Gutiérrez, C.A., Santoyo, M.A., Domínguez, J., Barrón, R., 1999. Tectonic implications of the earthquake swarm of 1997 in the Michoacán Triangle, Mexico. Journal of South American Earth Sciences 12, 567–577.

Pardo, M., Suárez, G., 1995. Shape of the subducted Rivera and Cocos plates in Southern Mexico: seismic and tectonic implications. Journal of Geophysical Research 100, 12357–12373.

Renne, P.R., Sharp, W.D., Deino, A.L., Orsi, G., Civetta, L., 1997. $^{40}Ar/^{39}Ar$ dating into the historical realm: calibration against Pliny the younger. Science 277, 1279–1280.

Siebe, C., Komorowski, J.C., Sheridan, M.F., 1992. Morphology and emplacement of an unusual debris avalanche deposit at Jocotitlán volcano, Central Mexico. Bulletin of Volcanology 54, 573–589.

Siebert, L., 1984. Large volcanic debris avalanches: characteristics of source areas, deposits, and associated eruptions. Journal of Volcanology and Geothermal Research 22, 163–197.

Singer, B.S., Thompson, R.A., Dungan, M.A., Feeley, T.C., Nelson, S.T., Pickens, J.C., Brown, L.L., Wulff, A.W., Davidson, J.P., Metzger, J., 1997. Volcanism and erosion during the past 930 k.y.

at the Tatara-San Pedro complex, Chilean Andes. Geological Society of America Bulletin 109, 127–142.

Stoopes, G.R., Sheridan, M.F., 1992. Giant debris avalanches from the Colima Volcanic Complex, Mexico: Implications for long-runout landslides (>100 km) and hazard assessment. Geology 20, 299–302.

Thouret, J.C., Finizola, A., Fornari, M., Legeley-Padovani, A., Suni, J., Frechen, M., 2001. Geology of El Misti volcano near the city of Arequipa, Peru. Geological Society of America Bulletin 113 (12), 1593–1610.

Urrutia-Fucugauchi, J., Flores-Ruiz, J.H., 1996. Bouguer gravity anomalies and regional crustal structure in central Mexico. International Geology Review 38, 176–194.

Wright, C.A., 1998. The AD 930 long-runout Round Top debris avalanche, Westland, New Zealand. New Zealand Journal of Geology and Geophysics 41, 493–497.